Research in Astronomy and Astrophysics, 22:105002 (13pp), 2022 October https://doi.org/10.1088/1674-4527/ac846b


# Study on the Influencing Factors of the Permittivity Estimation Method Considering Antenna Layout Based on Lunar Penetrating Radar

Rui-Gang Wang[1,2,3], Yan Su[1,2], Zong-Yu Zhang[1,2], Qing Zhang[1,2], Chen-Di Liu[1,2], Tian-Sheng Hong[1,2], Shu-Ning Liu[1,2], Wei Du[1,2], Shun Dai[1,2], Chun-Yu Ding[4], and Chun-Lai Li[1,2]

[1] National Astronomical Observatories, Chinese Academy of Sciences, Beijing 100101, China; suyan@nao.cas.cn

[2] School of Astronomy and Space Science, University of Chinese Academy of Sciences, Beijing 100049, China

[3] The 54th Research Institute of China Electronics Technology Group Corporation, Shijiazhuang 050081, China

[4] Institute of Moon-base Exploration and Observation, Institute of Advance Study, Shenzhen University, Shenzhen 518060, China

*Received 2022 February 11; revised 2022 July 11; accepted 2022 July 21; published 2022 September 15*

## Abstract

The permittivity of lunar regolith is crucial for further processing and interpretation of radar data. The conventional hyperbolic fitting method ignores the antenna height and spacing and has a significant error at a shallow depth. For the new method that considers the layout of the antenna, the influencing factors have not been studied. In this paper, we studied the influence of the position of the hyperbola peak and time zero on the new method for permittivity derivation. The simulation results show that when the input errors of time zero, abscissa and ordinate of the hyperbolic peak are $\pm 2$ ns, $\pm 0.02$ m and $\pm 0.2$ ns respectively, the average errors of the calculated results by points within 1 m from the hyperbolic peak are 10.0%, 16.7% and 38.2%, respectively. To improve the accuracy, we used the average results by points that are horizontally more than 1 m away from the hyperbola peak. Hence, we calculated the permittivity of the lunar regolith by the new method based on Lunar Penetrating Radar data. The average permittivity of the lunar regolith is estimated to be $3.3 \pm 1.2$.

*Key words:* Moon – techniques: radar astronomy – techniques: image processing

## 1. Introduction

In 2019, when Chang'E-4 landed in the Von Kármán impact crater on the farside of the Moon (as shown in Figure 1), it was the first time for human beings to do in situ exploration on the lunar farside (Li et al. 2019; Lai et al. 2019; Li et al. 2020; Dong et al. 2021; Wang et al. 2021). The Von Kármán crater is located in the South Pole-Aitken Basin (SPA), which was formed around 4.26 Ga ago (Huang et al. 2018). The maximum elevation difference of SPA is about 15 km. After the formation of the SPA crater, a large number of impacts reshaped the SPA surface (Huang et al. 2018; Lin et al. 2019). The lower lunar crust and the upper lunar mantle materials were excavated and ejected to the lunar surface (Li et al. 2020). Investigation of the SPA region is of great significance to study the origin of the Moon and the evolution of the solar system.

Due to the long-term impact of the meteorite, cosmic ray radiation, and the temperature difference between day and night on the Moon, the rocks and basalt lava on the lunar surface will be broken into fine particles. The older the geological age is, the deeper the lunar regolith (McKay et al. 1991; Lucey et al. 2000; Shkuratov & Bondarenko 2001; Zhang et al. 2015). The study of lunar regolith is helpful to study the geological activities and geological history of the lunar surface (Fa & Wieczorek 2012).

Chang'E-4 is composed of a lander and a rover. The payloads of Yutu-2 include a Panoramic Camera, Visible and Near-Infrared Imaging Spectrometer, Advanced Small Analyzer for Neutrals, and Lunar Penetrating Radar (LPR). LPR is designed to obtain the lunar regolith thickness and the subsurface structure (Jia et al. 2018). The LPR has two channels: high-frequency and low-frequency. There are two high-frequency receivers, Channel-2A and Channel-2B. The center frequency of the high-frequency channel is 500 MHz, and the lunar subsurface structure within more than 30 m depth can be obtained. The parameters of Channel-2B are shown in Table 1 (Fang et al. 2014; Su et al. 2014).

To obtain the regolith thickness and the subsurface structure, permittivity is required. The traditional hyperbola fitting method ignores the antenna height and spacing (Feng et al. 2017; Wang et al. 2021). The shallower the depth is, the greater the error (Wang et al. 2021). Wang et al. (2021) considered the influence of antenna spacing and antenna height and established a new model using geometric relations and time delay. The influencing factors and applicability are not studied. In this paper, the new method is further analyzed and verified. Finally, we use the new method to calculate the permittivity of the lunar regolith based on LPR data.

## 2. Method

### 2.1. Traditional Hyperbola Fitting Method

Yutu-2 is a rover, which is telemetered and controlled by ground commands. To facilitate traverse and avoid being

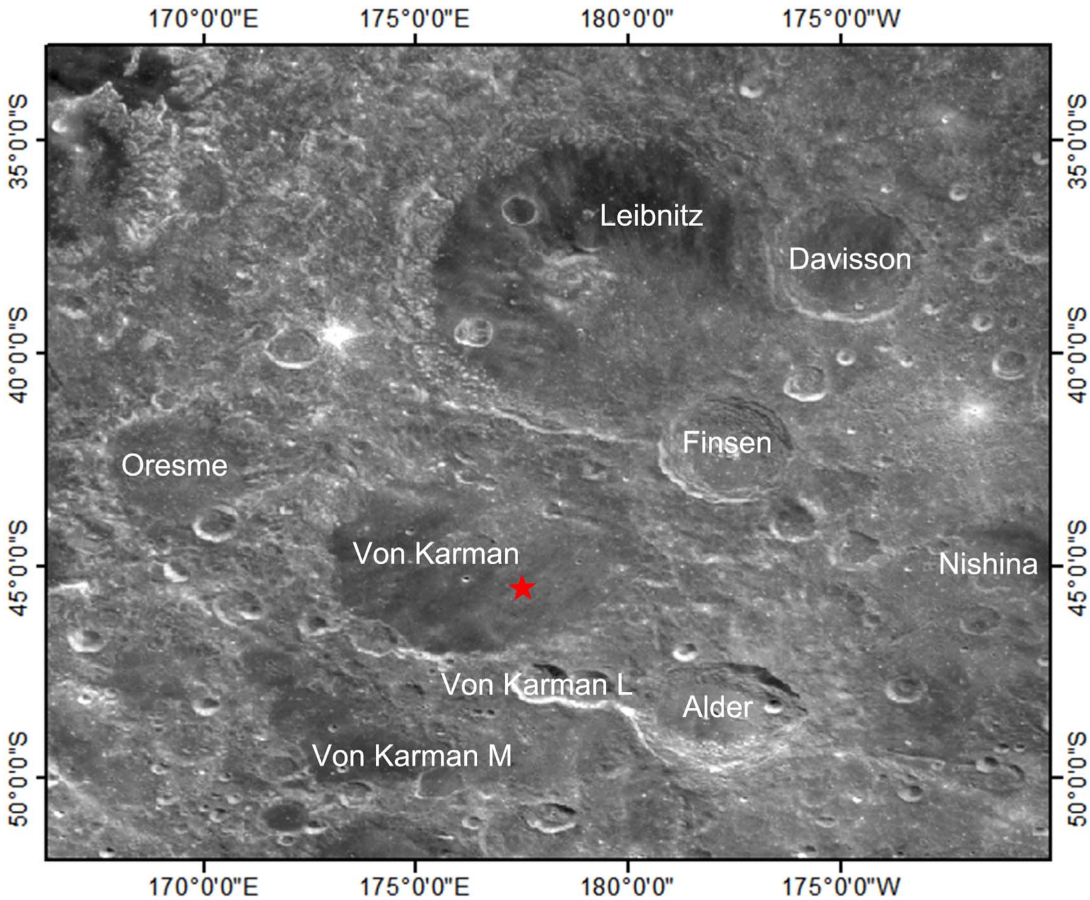


**Figure 1.** The geological background of the Chang'E-4 landing site. The red star indicates the landing site. The ID of the base image is CE1_GRAS DOM_120m_001_GLOBAL_A, which is available on the website (https://moon.bao.ac.cn/ce5web/searchOrder_dataSearchData.search).

blocked by obstacles such as lunar surface stones, the radar is suspended and installed at the bottom of Yutu-2 (as illustrated in Figure 2). The high-frequency antenna of LPR consists of three modules, one transmitting antenna and two receiving antennas. The height of the high-frequency antennas is about 0.3 m, and the spacing between antenna units is 0.16 m (Fang et al. 2014). The layout of the high-frequency antennas is drawn in Figure 2.

The traditional hyperbola fitting method ignores the influence of antenna height and spacing (Wang et al. 2021). As depicted in Figure 3, suppose the positions of the antenna and the reflector are $(x, 0)$ and $(x_0, H)$, and the permittivity and wave velocity are $\epsilon$ and $v$, respectively. The wave velocity in the lunar regolith can be expressed as (Fa et al. 2015; Dong et al. 2017, 2021; Feng et al. 2017)

$$v = \frac{c}{\sqrt{\epsilon}}, \tag{1}$$

where $c$ is the wave velocity in a vacuum.

**Table 1**
The Key Parameters Of Lunar Penetrating Radar

| Index | Parameter | Value |
|---|---|---|
| 1 | Centroid Frequency (MHz) | 500 |
| 2 | Sampling Rate (GHz) | 32 |
| 3 | Sampling Interval (ns) | 0.3125 |
| 4 | Antenna Height(2A) (cm) | 30 |
| 5 | Antenna Height(2B) (cm) | 30 |
| 6 | Antenna Spacing (cm) | 32 |
| 7 | Trace Interval (cm) | 3.65 |
| 8 | Range Resolution (cm) | $<30$ |
| 9 | Penetrating Depth (m) | $>30$ |

According to the geometric relation and time delay, the following equation can be derived.

$$t = \frac{2\sqrt{(x - x_0)^2 + H^2}}{v}, \tag{2}$$

where $t$ is the two-way travel time delay.

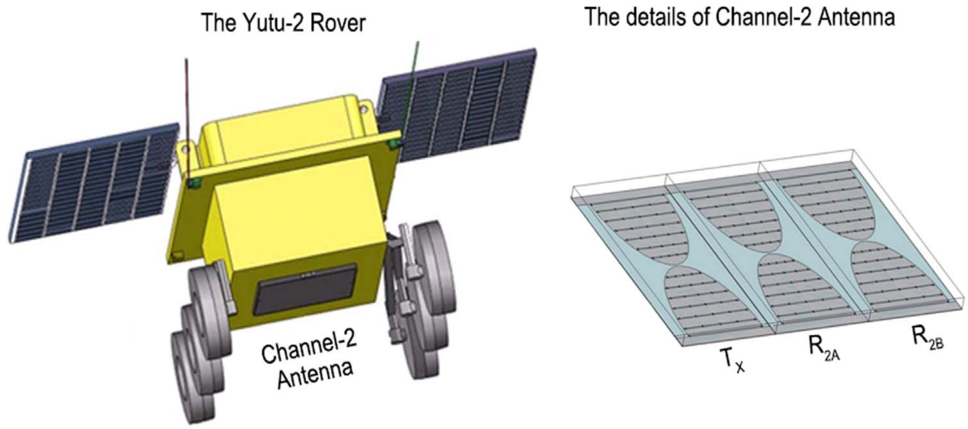


**Figure 2.** The schematic diagram of Yutu-2 and the Channel-2 antenna (Fang et al. 2014). $T_X$, $R_{2A}$ and $R_{2B}$ represent the transmitting antenna and the receiving antennas 2A and 2B, respectively.

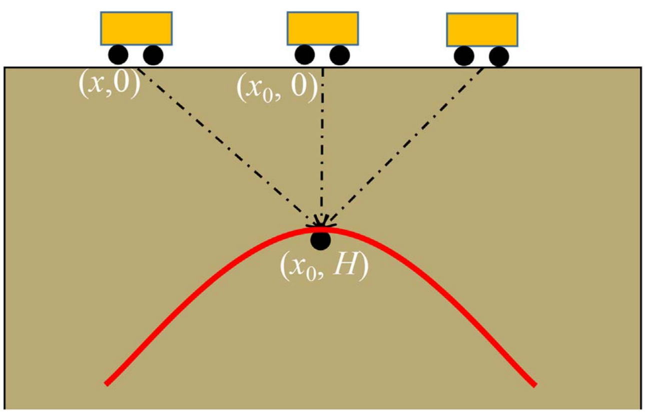


**Figure 3.** A schematic diagram of the hyperbola fitting method. The black circle is the reflector. The red solid curve is the reflected echo. The black dot-dashed lines indicate the propagation path when the antenna is at different positions.

As demonstrated in Figure 3, when there is a reflector in the regolith, a hyperbola is formed on the radargram (the red curve). The hyperbola can be detected on the radargram (Wang et al. 2021; Fa et al. 2015; Fa 2020; Lai et al. 2021), and the coordinates of the points on the hyperbola can be obtained. Hence, combined with Equation (2), the permittivity can be obtained by the curve fitting method (Feng et al. 2017; Ding et al. 2020, 2021; Wang et al. 2021).

### 2.2. Forward Modeling

As diagrammed in Figure 4, suppose the positions of the transmitter, receiver, reflector, incident point and emitting point are ($x$-$L/2$, $h$), ($x$+$L/2$, $h$), ($x_0$, -H), ($x_1$, 0) and ($x_2$, 0), respectively. According to the geometric relation, the time delay at different positions can be derived by the following equations (Wang et al. 2021).

$$\cdot = \frac{1}{\sqrt{\epsilon}}, \tag{3}$$

$$\cdot = \frac{1}{\sqrt{\epsilon}}, \tag{4}$$

$$\begin{aligned} &\sqrt{\epsilon}\left(\sqrt{H^2 + (x_0 - x_1)^2} + \sqrt{H^2 + (x_0 - x_2)^2}\right) \\ &+ \left(\sqrt{h^2 + \left(x - \frac{L}{2} - x_1\right)^2}\right. \\ &\left. + \sqrt{h^2 + \left(x + \frac{L}{2} - x_2\right)^2}\right) = c \cdot t, \end{aligned} \tag{5}$$

Based on the forward model above, we can obtain the theoretical time delay.

### 2.3. New Method For Permittivity Calculation

As affirmed in Figure 3, when the radar passes over the reflector, a hyperbola curve can be detected on the radargram. The horizontal distance $x$ and time delay $t$ of each point on the hyperbola can be obtained by picking points on the radargram. Suppose the coordinate of the hyperbola peak is ($x_0$, $t_0$). In Equations (3)–(5), there are five unknown variables in three equations, including $x_1$, $x_2$, $\epsilon$, $H$ and $x_0$. The equations are not solvable. To solve this problem, we have to find other relations to constrain the solution. Wang et al. (2021) proposed to utilize the geological and time delay relation when the antenna is directly above the reflector. As shown in Figure 5, suppose the radar is above the reflector, then the position of the antenna, reflector, incident point and ejection point are ($x$-$L/2$, $x$+$L/2$), ($x_0$, -$H$), ($x_1$, 0) and ($x_2$, 0), respectively. Equations (6) and (7) can be derived according to the geometric and time delay

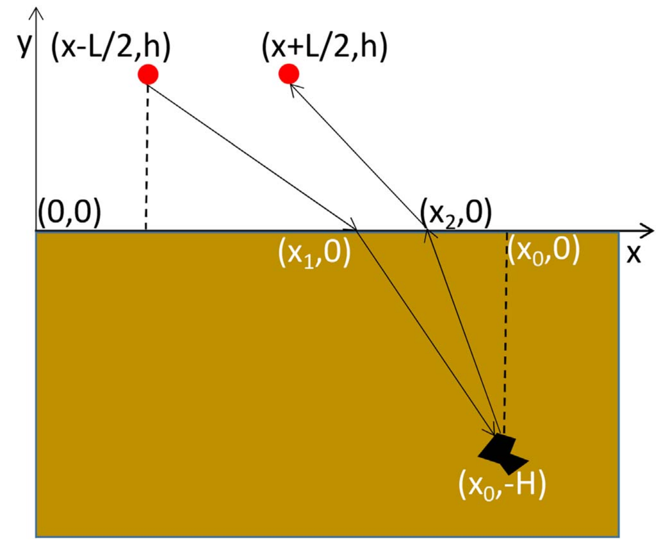


**Figure 4.** A schematic diagram of the wave propagation path when considering the antenna height and spacing.

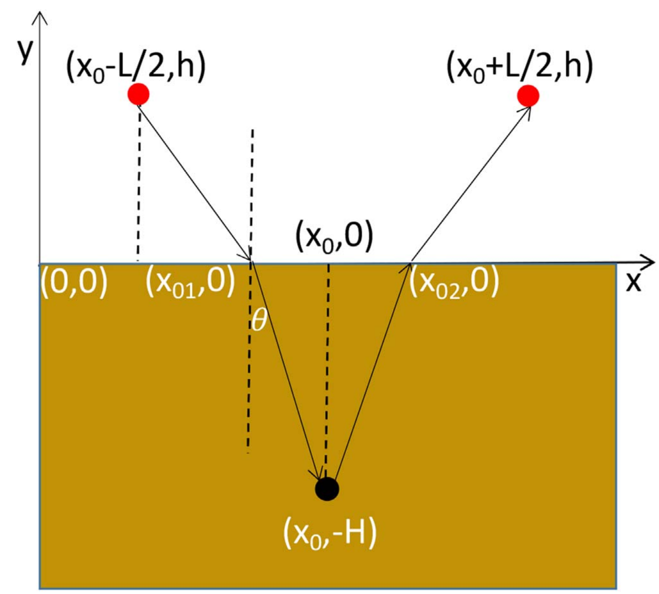


**Figure 5.** The wave propagation path of the new method when the antenna is above the reflector.

relation (Wang et al. 2021).

$$\frac{h\sqrt{\epsilon}\sin\theta}{\sqrt{1-\epsilon\sin^2\theta}} + H\tan\theta = \frac{L}{2}. \tag{6}$$

$$\frac{h}{\sqrt{1-\epsilon\sin^2\theta}} + H\frac{\sqrt{\epsilon}}{\cos\theta} = \frac{ct_0}{2}. \tag{7}$$

Combining Equations (3)–(7), there are seven unknown variables in five equations (as expressed in Equation (8)), including $x_1$, $x_2$, $\epsilon$, $H$, $\theta$, $x_0$ and $t_0$. Thus, the equations are not solvable. However, $(x_0, t_0)$ is the position of the peak of the hyperbola. $x_0$ can be determined by the symmetrical property of the hyperbola curve. $t_0$ is the minimum time delay of all points on the hyperbola curve, which can be determined manually (Wang et al. 2021). Therefore, there are five unknown variables ($x_1$, $x_2$, $\epsilon$, $H$, $\theta$) in five equations. The permittivity can be derived according to Equation (8).

$$\begin{cases} \text{-} = \dfrac{1}{\sqrt{\epsilon}}, \\ \text{-} = \dfrac{1}{\sqrt{\epsilon}}, \\ \dfrac{h\sqrt{\epsilon}\sin\theta}{\sqrt{1-\epsilon\sin^2\theta}} + H\tan\theta = \dfrac{L}{2}, \\ \dfrac{h}{\sqrt{1-\epsilon\sin^2\theta}} + H\dfrac{\sqrt{\epsilon}}{\cos\theta} = \dfrac{ct_0}{2}, \\ \sqrt{\epsilon}\left(\sqrt{H^2+(x_0-x_1)^2} + \sqrt{H^2+(x_0-x_2)^2}\right) \\ \quad + \left(\sqrt{h^2+\left(x-\dfrac{L}{2}-x_1\right)^2} + \sqrt{h^2+\left(x+\dfrac{L}{2}-x_2\right)^2}\right) = c\cdot t. \end{cases} \tag{8}$$

## 3. Result

### 3.1. The Forward Modeling Result

We established a regolith model with a depth and width of 12 m and 10 m, respectively. Suppose the reflector is horizontal in the middle of the model. The depths are set to be 1 m, 3 m, 5 m, 7 m, 9 m and 11 m respectively. The permittivity is 3. Using the forward model, the theoretical time delay of the reflected signal can be obtained. As affirmed in Figure 6, the curvature of the hyperbola decreases with the increase of the depth of the reflector.

### 3.2. The Influence Of The Estimation Error Of The Position Of The Hyperbola Peak

According to the principle of the new method, $(x_0, t_0)$, the position of the hyperbola peak is an input constant, which should be determined before solving Equation (8). The estimation error of $(x_0, t_0)$ may influence the new method. We applied the forward modeling simulation method to estimate the influence.

#### 3.2.1. The Influence Of The Estimation Error Of The Horizontal Distance Of The Hyperbola Peak

The position of the hyperbola peak is the input parameter of the new method. To study the influence of the estimation error of the horizontal distance ($x_0$) of the hyperbola peak on the calculated permittivity, we input $x_0$ with different errors. Suppose $x_0$ is the theoretical value, then the estimation errors

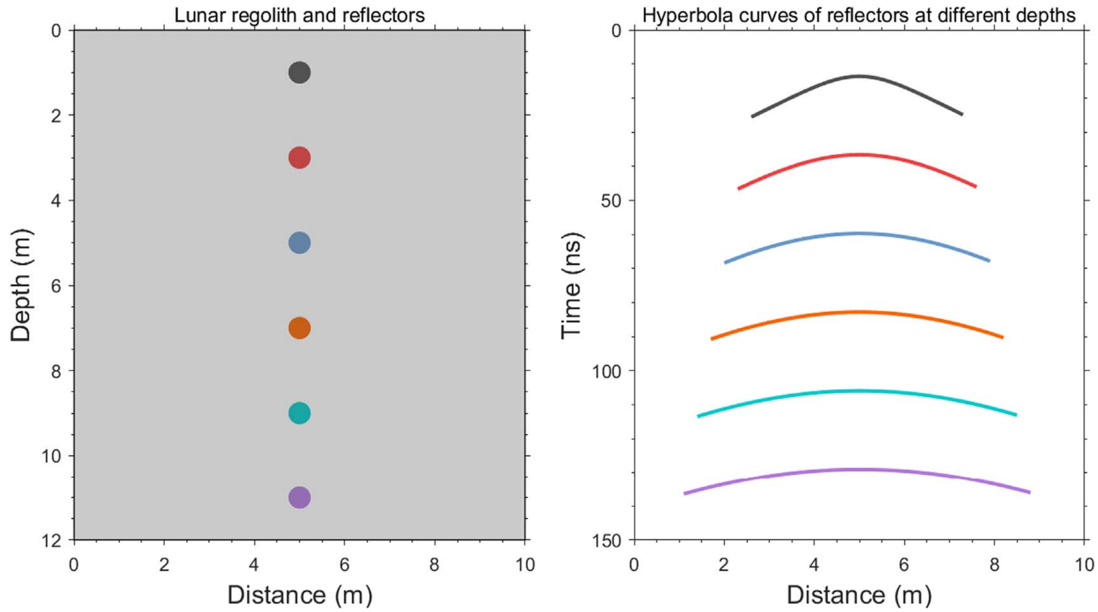


**Figure 6.** The position of the reflectors and the corresponding hyperbola curve.

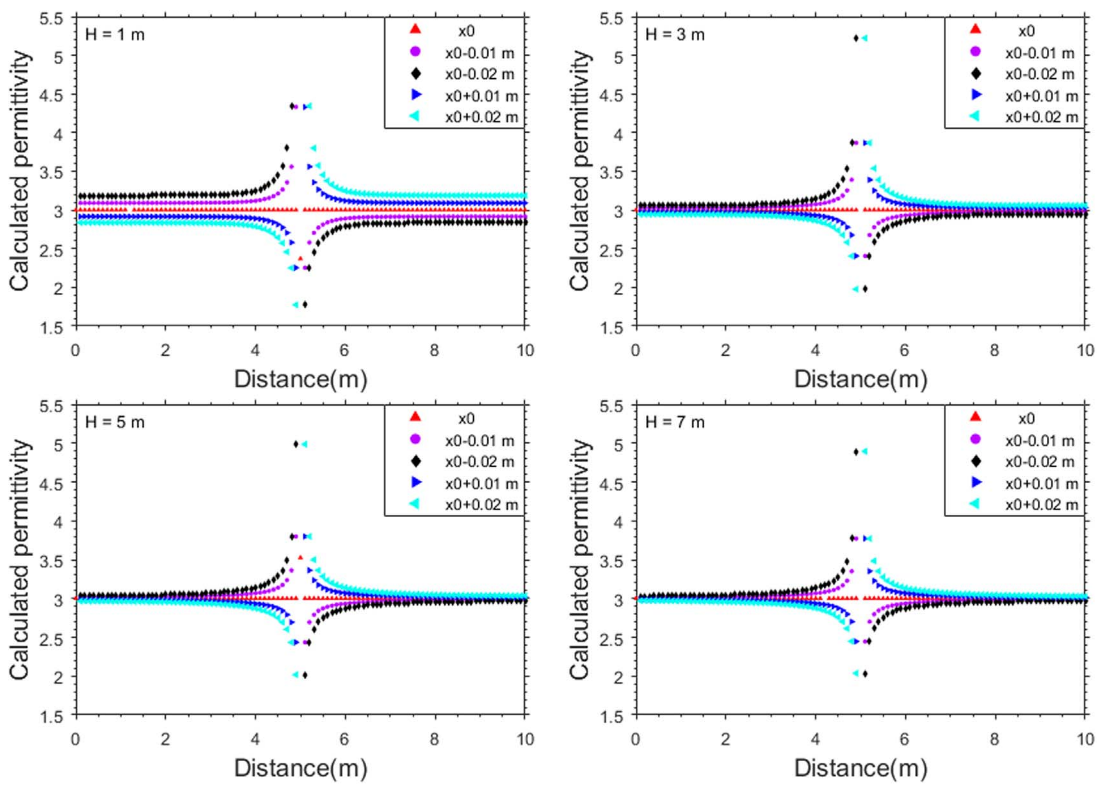


**Figure 7.** The estimated permittivity at different depths with different $x_0$ discrepancy. $x_0$ is the horizontal distance of the peak of the hyperbola, which is used for further calculation in the new method.

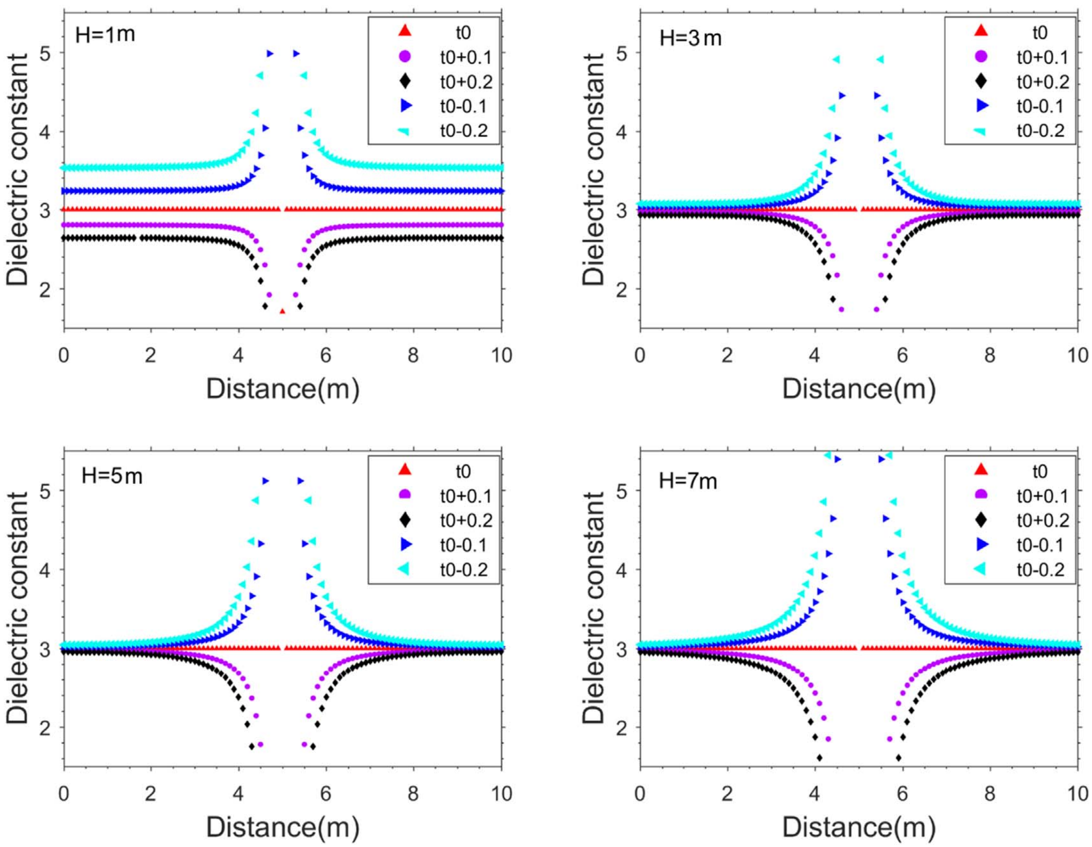


**Figure 8.** The estimated permittivity at different depths with different $t_0$ discrepancy. $t_0$ is the time delay of the peak of the hyperbola, which is used for further calculation in the new method.

**Table 2**
Average Relative Error Of Derived Permittivity Caused By The Estimation Error of $x_0$

| Error Range of $x_0$ | Distance from the Hyperbola Peak | |
|---|---|---|
| | >1 m | ⩽1 m |
| ±0.01 m | 1.5% | 7.7% |
| ±0.02 m | 3.0% | 16.7% |

are ±0.01 m and ± 0.02 m. The depth of the reflector is set to be 1 m, 3 m, 5 m and 7 m. The result is shown in Figure 7.

As displayed in Figure 7, the shallower the depth of the reflector is, the larger the estimation error of permittivity. Moreover, the closer the selected point is to the hyperbola peak, the greater the error. To further analyze the effect of the horizontal distance of the hyperbola peak ($x_0$), we quantified the error of the results obtained at various depths. The result is expressed in Table 2. As shown in Table 2, the relative errors are obvious when the selected point on the hyperbola is in the range of 1 m from the hyperbola peak. The average relative errors are 7.7% and 16.7% when the errors of $x_0$ are ±0.01 m and ±0.02 m, respectively. The relative error of the results by points that are more than 1 m from the hyperbola peak is within 5%.

### *3.2.2. The Influence Of The Estimation Error Of The Time Delay Of The Hyperbola Peak*

Like the process of the analysis of $x_0$, we set different input errors to analyze the influence of the estimation error of $t_0$. The result is plotted in Figure 8. As displayed in Figure 8, the smaller $t_0$ is, the larger the estimated permittivity. In addition, like the result in Figure 7, the estimated permittivity near the hyperbola peak shows great deviation. The permittivity obtained by the new method should be the average of the results except for the points too close to the hyperbola peak. Table 3 demonstrates the average error of calculated permittivity with different input errors of $t_0$ within different distance ranges. When the input errors of $t_0$ are ±0.1 ns and ±0.2 ns, the errors of the calculated permittivity by points within 1 m from the hyperbola peak are 28.6% and 38.2% respectively. The error of calculated permittivity by points with a distance of more than 1 m from the hyperbola peak is less than 5%.

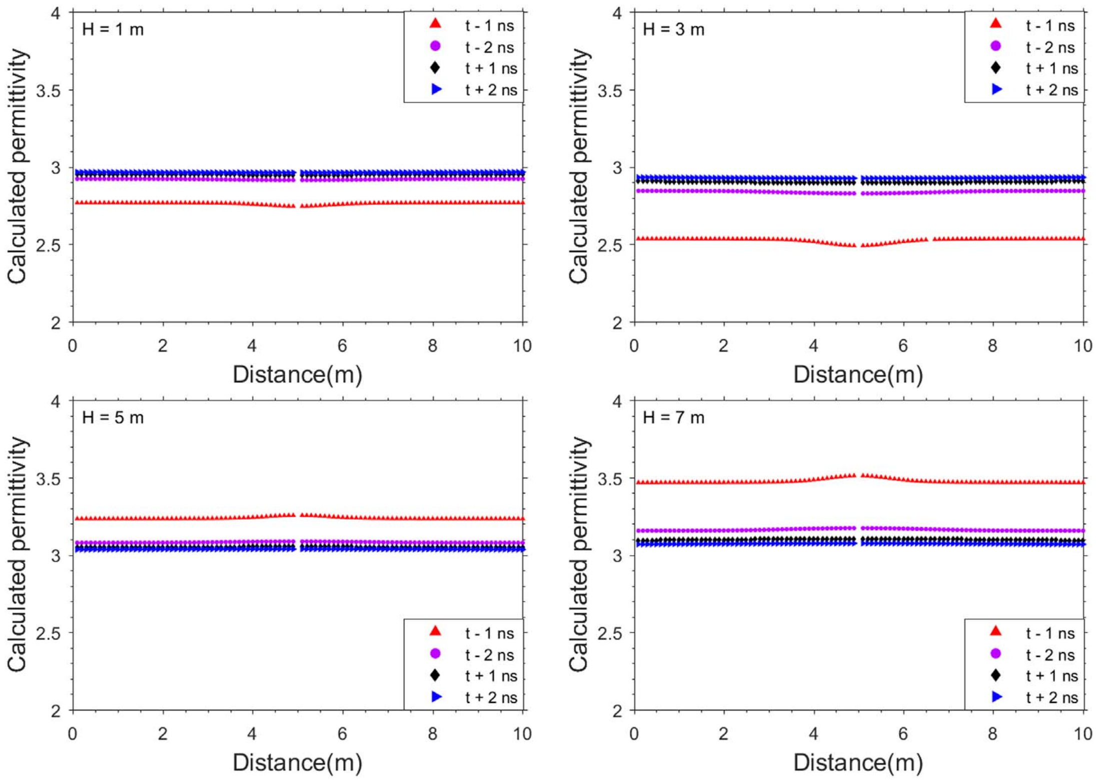


**Figure 9.** The influence of time zero on the new method.

**Table 3**
Estimation Error Caused By The Error Of $t_0$

| Error Range of $t_0$ | Distance from the Peak | |
|---|---|---|
| | >1 m | ⩽1 m |
| ±0.1 ns | 2.6% | 28.6% |
| ±0.2 ns | 4.9% | 38.2% |

**Table 4**
Estimation Error Caused By The Error Of Time Zero

| cc Error Range of Time Delay | Distance from the Peak | |
|---|---|---|
| | >1 m | ⩽1 m |
| ±1 ns | 3.3% | 7.4% |
| ±2 ns | 6.7% | 10.0% |

### *3.3. The Influence Of Time Zero*

Time zero adjustment is an indispensable step in radar data processing. Accurate determination of zero time is crucial to radar signal processing and interpretation (Zhang et al. 2018). Like the analysis of $x_0$, we input time zero with different errors when deriving permittivity (±1 ns and ±2 ns). The depth of the reflectors is set to be 1 m, 3 m, 5 m and 7 m. The results are shown in Figure 9. As affirmed in Figure 9, when the reflector is at a shallow depth, the calculated permittivity is proportional to the time delay. The smaller the time delay is, the smaller the estimated permittivity. When the reflector is at a deep depth, the calculated permittivity is inversely proportional to the time delay. The smaller the time delay is, the larger the estimated permittivity. The quantitative analysis of the influence of time zero is shown in Table 4. When the input errors of time zero are ±1 ns and ±2 ns, the errors of the calculated permittivity by points within 1 m from the hyperbola peak are 7.4% and 10% respectively. The error of calculated permittivity by points with a distance of more than 1 m from the hyperbola peak is slightly more than 5%.

### *3.4. The Permittivity of Lunar Regolith At The Chang'E-4 Landing Site*

Chang'E-4 landed on the farside of the Moon on 2019 Jan. 3. We calculated the permittivity of lunar regolith by the new method with the LPR data of the first 30 lunar days. Due to the uneven traverse speed in some areas and the radar being off in some areas, the hyperbolas in these areas are deformed (as displayed in Figures 10(a)–(e)). In addition, from the analysis of the influence of the position of the hyperbolic peak, it can be seen that when selecting points on the hyperbola, there will be

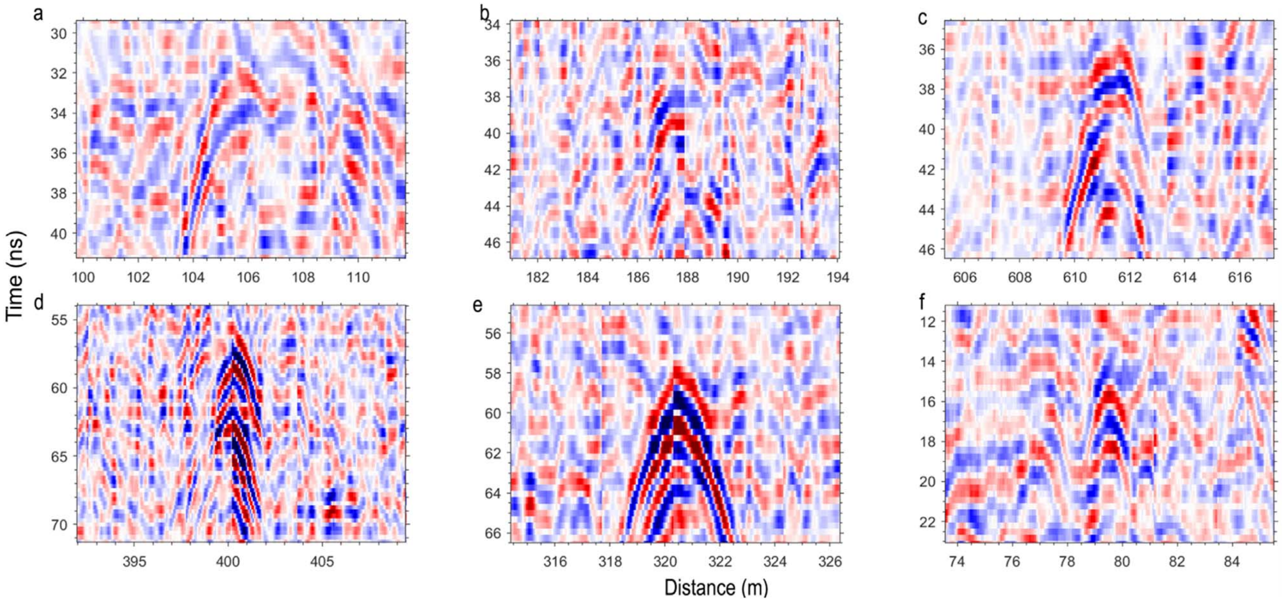


**Figure 10.** Examples of some hyperbola curves not available for calculation.

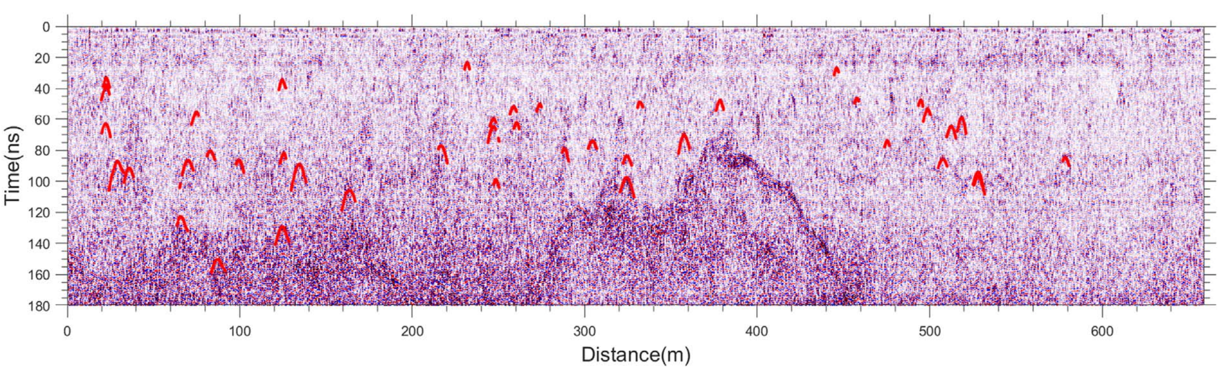


**Figure 11.** The selected hyperbola curves on the radargram. The red lines indicate the position of the selected hyperbola.

obvious errors when the points are close to the middle of the hyperbola. As shown in Figure 10(f), at the shallower depth, the hyperbola curve is very short, and the points on the hyperbola curve are close to the middle of the hyperbola, which may lead to errors. The selected hyperbola curves are depicted in Figure 11, in which the red curves represent the selected hyperbolas. The calculated result is plotted in Figure 12. The average permittivity of the lunar regolith within the first 30 lunar days is estimated to be $3.3 \pm 1.2$.

## 4. Discussion

### *4.1. Properties Of The Hyperbola Fitting Method and The Proposed Method*

The new method is based on the geometric and time delay relation when the radar is directly above and obliquely above the reflector. The permittivity is obtained by solving equations. When the radar is close to the top of the reflector, the difference between the two cases (the radar is directly above and obliquely above the reflector) is not obvious, and the constraint conditions of the equations are insufficient. Therefore, the equations are not stable. Moreover, due to the small height and spacing of the antenna, there is a certain error in the calculation process. These factors will make the error increase sharply when the radar approaches the top of the reflector. To improve the accuracy, the calculation results of points close to the hyperbola peak should be removed. The final calculation result should be the average of the calculation results of the points away from the hyperbola peak.

The traditional hyperbola fitting method is based on the simplified model which ignores the antenna height and spacing. The calculation error of the traditional hyperbola fitting method

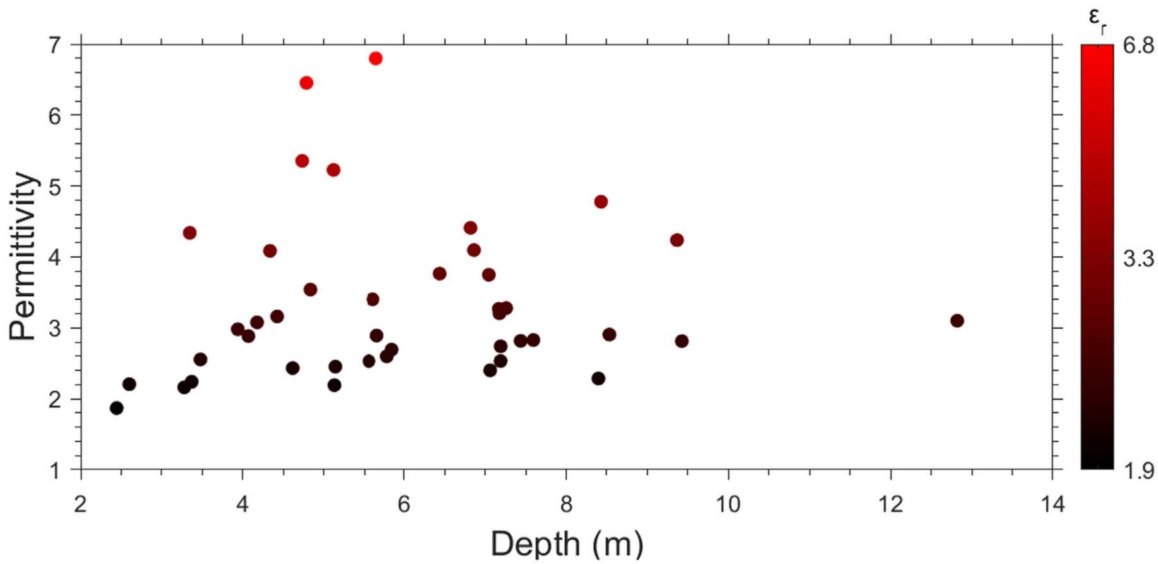


**Figure 12.** The permittivity calculated at different depths.

increases with the decrease of depth. The error is mainly caused by the simplified model (Wang et al. 2021). When the reflector is at a deep depth, the antenna height and spacing are smaller compared to the depth of reflectors. The error caused by the simplified model can be ignored. However, when the reflector is at a shallower depth, the influence of the antenna height and spacing is obvious. Consequently, the results obtained by the traditional method at the shallow depth have large errors, and the errors at the deep depth are small.

### *4.2. The Influence Of The Horizontal Distance Of The Hyperbola Peak*

The position of the hyperbola peak ($x_0$, $t_0$) is an important input constant for the new method. For a certain hyperbola curve, $x_0$ and $t_0$ are used in the estimation of the permittivity for each picked point. Therefore, obtaining the position of the hyperbola peak accurately is essential for the new method.

Figure 13 illustrates the wave paths of reflectors with different horizontal distances. To simplify the analysis, only the down-going wave is shown. Suppose A is the theoretical position, and A1 and A2 are the estimated positions with horizontal distances smaller and larger than the theoretical value respectively. As depicted in Figure 13(a), when the radar is on the upper left of the reflector, if $x_0$ is smaller than the theoretical value (A1), the wave path becomes longer (the blue dashed line corresponding to A1 is compared with the red solid line corresponding to A), the derived wave velocity is smaller and the estimated permittivity is larger. On the other hand, when the horizontal distance of the hyperbola peak is larger (A2 in Figure 13), the permittivity is smaller. Likewise, when the radar is at the upper right of the reflector (Figure 13(b)), the situation is opposite to that at the upper left. Figure 7 shows the permittivity derived by different points on the hyperbola at different depths with different horizontal distance errors. The results are consistent with the analysis above. At the same time, it can be seen that the influence of horizontal distance error decreases with the increase of depth.

Accurate determination of the horizontal distance of the hyperbola peak is important for the new method. $x_0$ can be obtained by several methods, including manual selection, machine learning, curve fitting methods, etc. Manual selection is the most straightforward method, but the error is significant. The machine learning method can identify a hyperbola from a complex radargram, but it is a time-consuming process and requires a large training set. The hyperbolic fitting method is simple to implement and can obtain accurate results. Therefore, in this paper, we use the curve fitting method to obtain $x_0$.

### *4.3. The Influence Of The Time Delay Of The Hyperbola Peak*

The time delay ($t_0$) of the hyperbola peak represents the depth of the reflector. When the estimated $t_0$ is less than the theoretical value (A1 in Figure 14), the corresponding wave path becomes smaller, the estimated wave velocity becomes larger and the estimated permittivity becomes smaller. Likewise, when the estimated $t_0$ is greater than the theoretical value (as shown in A2 in Figure 14), the estimated permittivity becomes larger. As demonstrated in Figure 8, the smaller the time delay of the hyperbola peak ($t_0$) is, the larger the estimated permittivity. Meanwhile, the influence of $t_0$ decreases with the increase of depth.

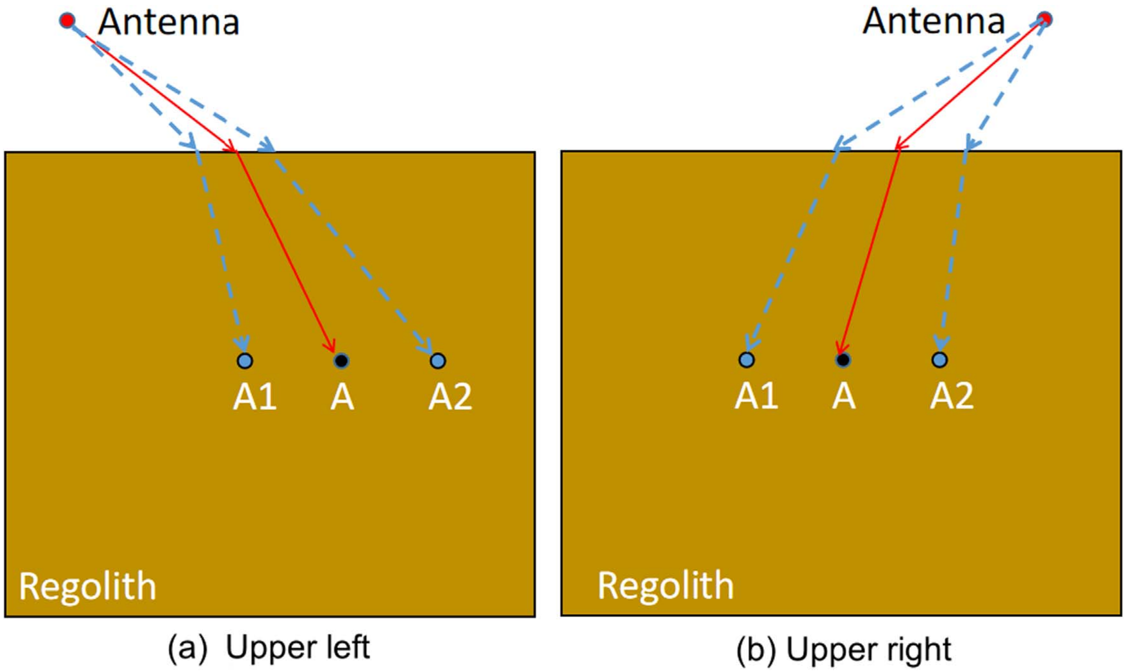


**Figure 13.** Wave paths of reflectors with different horizontal distance. (a), (b) The wave paths of reflectors when the antenna is on the upper left and right of the reflector respectively. The red line is the theoretical wave path, the blue dashed lines are the wave paths regarding the horizontal distances with errors. A is the theoretical position of the reflector, and A1 and A2 are the estimated positions.

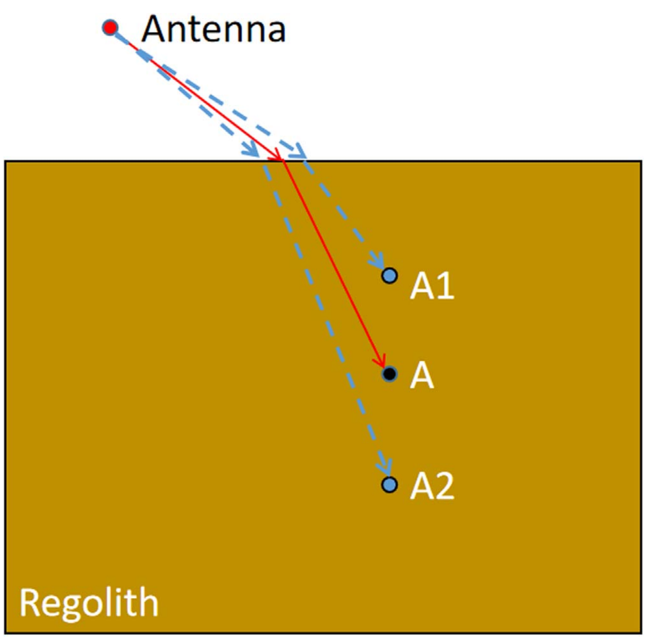


**Figure 14.** Wave paths of reflectors with different time delay of the hyperbola peaks. The red line is the theoretical wave path, and the blue dashed lines are the wave paths regarding the horizontal distances with errors. A is the theoretical position of the reflector, while A1 and A2 are the estimated positions.

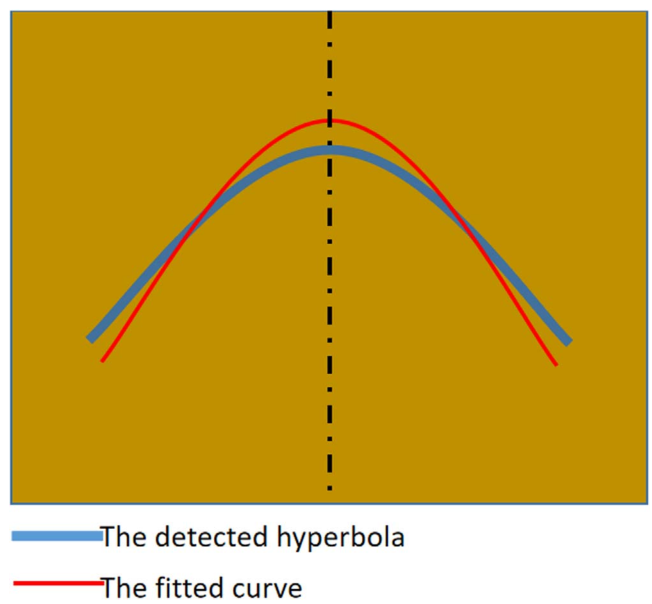


**Figure 15.** Schematic diagram of the detected hyperbola and the fitted curve. The blue line and red line indicate the detected hyperbola curve and the fitted curve respectively. The black dashed line represents the center of the hyperbola.

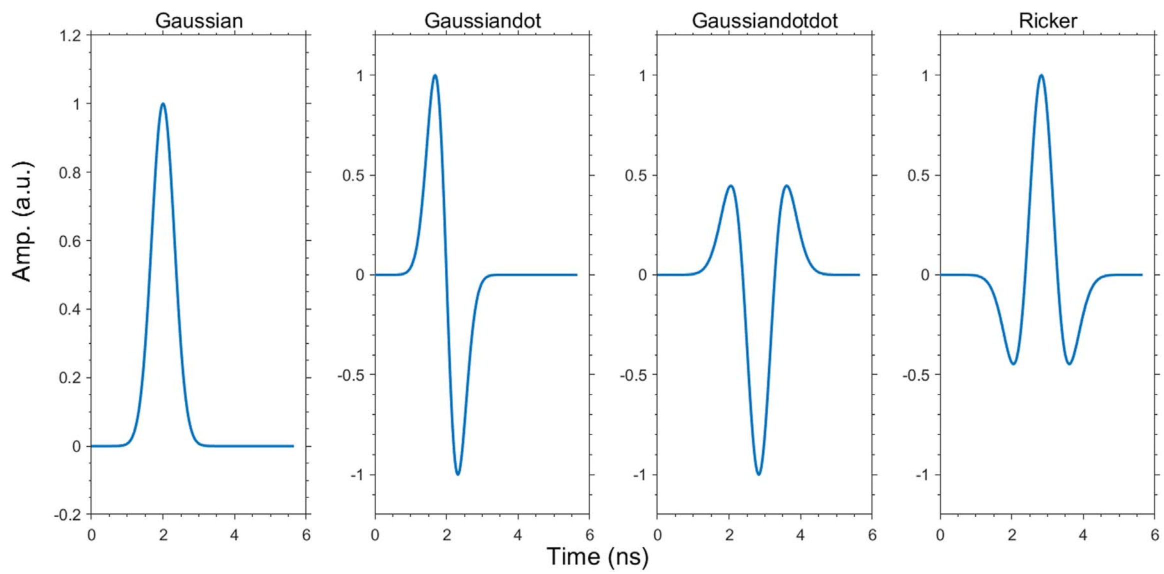


**Figure 16.** Waveform of different wavelets.

Figure 15 depicts a schematic diagram of the detected hyperbola and the fitted curve. Due to the simplified model of the hyperbola fitting method, which ignores the antenna height and spacing, the fitted curve and the detected curve do not coincide perfectly. The curve fitting method can accurately obtain the horizontal distance of the peak, but the derived time delay of the hyperbola peak is inaccurate. Therefore, $t_0$ cannot be accurately obtained by the curve fitting method. Compared to the curve fitting method, the manual method is more convenient and the result is more accurate. Thus, we used the manual pick method to obtain $t_0$.

### *4.4. The Influence Of Time Zero*

The radar transmitter transmits signals. When it encounters a reflector, it will generate a reflected signal to be received by the receiver. The time delay from the transmitter transmitting a signal to the receiver receiving the signal is related to the propagation distance. It is very important to accurately ascertain the time delay for determining the position of the reflector.

Due to the limitation of design and manufacturing technology, the actual radar signals cannot be the ideal impulse signal. The actual signal is wider than the impulse signal, which makes it difficult to determine the time delay. Figure 16 shows the common waveform used in the Ground Penetrating Radar (GPR) field, including the Gaussian, Gaussiandot, Gaussiandotdot and Ricker (Giannopoulos 2005). In the traditional GPR field, it roughly takes the position of the first negative peak as the time zero position, which is regarded as a benchmark to determine the time delay of the reflected signals. This rough method of determining the time zero will result in errors.

To obtain the time delay more precisely, the phase relation of the coupling wave and the reflected echo can be exploited to determine the time delay. Figure 17(a) illustrates the working principle of LPR radar, while Figure 17(b) features a schematic diagram of the received signal. The received signals include coupling wave, surface-reflected wave and underground-reflected wave, the positions of which are marked by A, B and C, respectively. A’ indicates the position of the time zero. The time from A’ to A is the time interval from when the signal is transmitted by the transmitter to when it is directly received by the receiver. Therefore, the time from A’ to C is the time delay of the underground-reflected signal.

The position of the reflected signal should be determined according to the waveform. As shown in Figure 17, here, we only take the Ricker wavelet as an example. The position of the coupling wave (A) is particularly easy to be identified. Hence, the time delay from the transmitter to the receiver can be determined according to the antenna layout, so that the position of time zero (A’) can be obtained.

### *4.5. The Selection Of The Hyperbola Curves*

Due to the aperture of the radar system, a hyperbola will be formed on the radargram when the radar passes over reflectors buried in the lunar regolith. The properties of the hyperbola are related to the permittivity of the lunar regolith. The permittivity can be derived by the properties of the hyperbola. A hyperbola is the basis of both traditional and new methods to calculate permittivity. Due to the influence of low resolution, noise, uneven channel spacing, etc., some of the hyperbolas on the

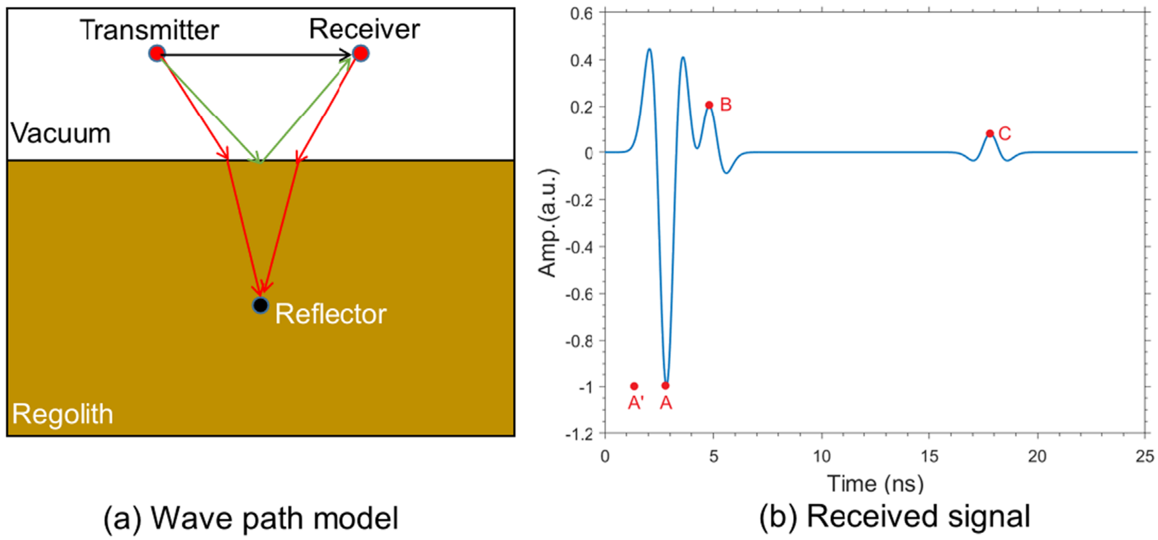


**Figure 17.** Schematic diagram of the received signal. A', A, B and C indicate the position of the time zero, coupling wave, surface-reflected wave and underground-reflected wave, respectively.

radargram will be disturbed, and there is a large error in the calculated permittivity. Therefore, it is essential to select effective hyperbolas. In the practical process, the manual pick method is widely used in the GPR and LPR field, which is influenced by subjective factors. When selecting a hyperbola, attention should be paid to the following aspects: (1) the velocity of the rover should be uniform. The uniform velocity makes the trace spacing uniform. Low velocity results in data redundancy and small curvature of the hyperbola. The calculated permittivity is smaller than the theoretical value. On the other hand, high velocity will result in data loss and large curvature of the hyperbola. The calculated permittivity is larger than the theoretical value. (2) Avoid the data combination errors. Due to the detection requirements of other payloads, when the rover travels to a specific area, it needs to stop moving for tasks like taking photos, spectral analysis, etc., but the radar is still on. During this period, a large number of duplicated data are obtained, which need to be removed. This process is completed manually, so it may cause residue of duplicated data or loss from moving the data. These will lead to the horizontal distance error of the points on the hyperbola, resulting in the curvature change of the hyperbola, which will affect the derived permittivity. (3) For the new method, the derived permittivity by the points on the hyperbola within one meter from the hyperbola peak has a large error. Therefore, when selecting hyperbolas, hyperbolas with a width greater than 2 m should be selected.

## 5. Conclusion

The antenna of the LPR is mounted above the ground. The height and spacing of the antenna will affect the permittivity derivation results. We analyzed the influencing factors of the new method for permittivity derivation, which considers antenna height and spacing. Simulation results show that the relative errors caused by these factors can reach 10%–38% within 1 m around the hyperbola peak. To improve the estimation accuracy, we used points on the hyperbola curve that have a horizontal distance of more than 1 m from the hyperbola peak for calculation. Hence, we calculated the permittivity of the lunar regolith by the new method based on LPR data of the first 30 lunar days. The results obtained by the new methods are about $3.3 \pm 1.2$.

## Acknowledgments

This work was funded by the National Natural Science Foundation of China (NSFC, Grant No. 12073048), and supported by the Key Research Program, Chinese Academy of Sciences, Grant No. ZDBS-SSW-JS007.

## ORCID iDs

Rui-Gang Wang https://orcid.org/0000-0001-8219-6876
Chen-Di Liu https://orcid.org/0000-0002-1767-8219

## References

Ding, C., Cai, Y., Xiao, Z., & Su, Y. 2020, Earth Planets. Phys., 4, 105
Ding, C., Xiao, Z., Su, Y., & Cui, J. 2021, Icar, 358, 114280
Dong, Z., Fang, G., Ji, Y., et al. 2017, Icar, 282, 40
Dong, Z., Fang, G., Zhou, B., et al. 2021, JGRE, 126, e2020JE006564
Fa, W. 2020, Earth Space Sci., 7, e2019EA000801
Fa, W., & Wieczorek, M. A. 2012, Icar, 218, 771
Fa, W., Zhu, M.-H., Liu, T., & Plescia, J. B. 2015, GeoRL, 42, 10
Fang, G.-Y., Zhou, B., Ji, Y.-C., et al. 2014, RAA, 14, 1607

Feng, J., Su, Y., Ding, C., et al. 2017, Icar, 284, 424
Giannopoulos, A. 2005, Constr. Build. Mater., 19, 755
Huang, J., Xiao, Z., Flahaut, J., et al. 2018, JGRE, 123, 1684
Jia, Y., Zou, Y., Ping, J., et al. 2018, P&SS, 162, 207
Lai, J., Cui, F., Xu, Y., Liu, C., & Zhang, L. 2021, RemS, 13, 4056
Lai, J., Xu, Y., Zhang, X., et al. 2019, GeoRL, 46, 12783
Li, C., Liu, D., Liu, B., et al. 2019, Natur, 569, 378
Li, C., Su, Y., Pettinelli, E., et al. 2020, SciA, 6, eaay6898
Lin, H., He, Z., Yang, W., et al. 2020, Natl Sci. Rev., 7, 913
Lucey, P. G., Blewett, D. T., Taylor, G. J., & Hawke, B. R. 2000, JGRE, 105, 20377
McKay, D. S., Heiken, G., Basu, A., et al. 1991, Lunar Source Book, Vol. 567 (Cambridge: Cambridge Univ. Press), 285
Shkuratov, Y. G., & Bondarenko, N. V. 2001, Icar, 149, 329
Su, Y., Fang, G.-Y., Feng, J.-Q., et al. 2014, RAA, 14, 1623
Wang, R., Su, Y., Ding, C., et al. 2021, RemS, 13, 3679
Zhang, J., Yang, W., Hu, S., et al. 2015, PNAS, 112, 5342
Zhang, L., Zeng, Z., Li, J., et al. 2018, Senso, 18, 2907